ELSEVIER

Journal of Crystal Growth 237–239 (2002) 149–153

JOURNAL OF CRYSTAL GROWTH

www.elsevier.com/locate/jcrysgro

History effects during the selection of primary dendrite spacing. Comparison of phase-field simulations with experimental observations

H.-J. Diepers*,[1], D. Ma, I. Steinbach

ACCESS eV RWTH, Intzestrasse 5, 52072 Aachen, Germany

Abstract

The paper describes numerical experiments to investigate the selection of primary dendritic spacing λ under transient conditions. The phase field method coupled to solutal diffusion is combined with a moving frame algorithm to enlarge the total calculation domain. For constant growth conditions of an Al–7%Si alloy, a range of λ has been achieved depending on initial conditions. Quasistationary decrease of the solidification velocity leads to extinction of redundant trunks. Increasing the velocity leads to the formation of new trunks from ternary arms, but a striking incubation delay suggests a history-dependent spacing assignment. The results are compared to experimental and theoretical results.

Keywords: A1. Computer simulation; A1. Dendrites; A1. Directional solidification; A1. Phase field

1. Introduction

In materials microstructure classification the primary spacing λ of dendritic arrays is a key factor, which is controlled mainly by the solidification speed. For decreasing velocities, the overlapping solutal diffusion fields select out redundant dendrite trunks, while for increasing velocities smaller spacings are achieved through the "birth" of new dendrites from ternary arms. In classical theories [1,2] an unique spacing is determined as function of the solidification parameters [3]. The e.g., proposed for steady state is

$$\lambda = 2\pi(kD\Gamma\,\Delta T_0)^{1/4} G^{-1/2} V^{-1/4} \tag{1}$$

with the coefficients for partition k, diffusion D, Gibbs–Thomson curvature Γ, solidification interval ΔT_0, temperature gradient G and solidification speed V. Experimental results and more sophisticated theoretical models [4,5] indicate a continuous range of states. Finally, [6–8] it was realized that even the average spacing remarkably depends on the history of the evolution and selection. A hysteresis like delay can be observed for increasing/decreasing velocities.

Phase field models are able to model dendritic solidification. Several models couple the phase-field approach with solutal fields [9–12]. The applied model here [9] avoids jumps of the chemical potential across the interface and has

*Corresponding author. Tel.: +49-241-80-98000; fax: +49-241-38578.

E-mail address: h.diepers@access.rwth-aachen.de (H.-J. Diepers).

[1] url: http://www.access.rwth-aachen.de

0022-0248/02/$ - see front matter
PII: S0022-0248(01)01932-7

advantages in its pragmatic applicability to multi-phase multi-component systems.

In any model there remain problems caused by artificial solute trapping, interface spreading, etc. described mathematically in Ref. [13], which actually are promised to get solved by Ref. [14].

2. Simulation model

The phase-field equation used here is one of the special cases given in Ref. [9], it is also derived in Ref. [16] and reads as

$$\frac{\mathrm{d}\phi}{\mathrm{d}t} = \mu\Gamma[\nabla^2\phi - 36\phi(1-\phi)(1-2\phi)/\delta^2] - [T - T_\mathrm{m} - m_\mathrm{l}\langle c_\mathrm{l}\rangle]\,30/\delta\,\phi^2(1-\phi)^2 \quad (2)$$

and describes the evolution of the liquid/solid interface represented by the phase-field parameter, which continuously changes from liquid ($\phi = 0$) to solid ($\phi = 1$) within the interfacial layer δ. The coefficient μ describes the attachment kinetic, Γ is the Gibbs–Thomson coefficient and m_l is the liquidus slope.

The concentration equation is

$$\frac{\mathrm{d}c}{\mathrm{d}t} = \nabla D(\phi)[\nabla c - (c_\mathrm{l} - c_\mathrm{s})\,\nabla\phi, \quad (3)$$

where the first summand describes diffusion in the single phase domains with $D(\phi)$ changing with ϕ from D_liquid to D_solid. The latter is assumed to be zero in the actual calculations. The second term provokes a solubility jump due to phase-diagram data $c_\mathrm{l} - c_\mathrm{s}$ across the interface. c_l and c_s are recoupled to c by $c = c_\mathrm{l} - \varphi(c_\mathrm{l} - c_\mathrm{s})$. Equations for ϕ and c are solved with a standard control volume approach [15] on a rectangular grid.

Eqs. (2) and (3) are explicitly described in Ref. [16] and are special cases of Ref. [9], but the following changes in Eq. (2) have been introduced: for stability reasons the concentration $\langle c_\mathrm{l}\rangle$ was taken as average of c_l across the interface. Also the c_l coupled term $30\phi^2(1-\phi)^2$ stabilizes the interface against the original term $6\phi(1-\phi)$ in Refs. [9,15] comparable to the differences of model 1 against model 2 described in Ref. [17]. For the conditions of directional solidification the temperature was set across the calculation domain linearly according to the imposed temperature gradient decreasing with cooling rate $R = \mathrm{d}T/\mathrm{d}t$.

In order to economize calculation time we introduced a special moving frame of reference. As we are not interested in late stage phase transformations like ripening here, but in the evolution of primary spacing, it is sufficient to simulate only the relevant window of solutal supercooled liquid at the dendrite tips. The moving frame works digitally in magnitudes of the numerical grid: if a relevant temperature at the bottom of the domain is reached, then all grid variables were indexed one z-coordinate lower. The rows introduced new into the domain (from the upper side) were initialized with fixed

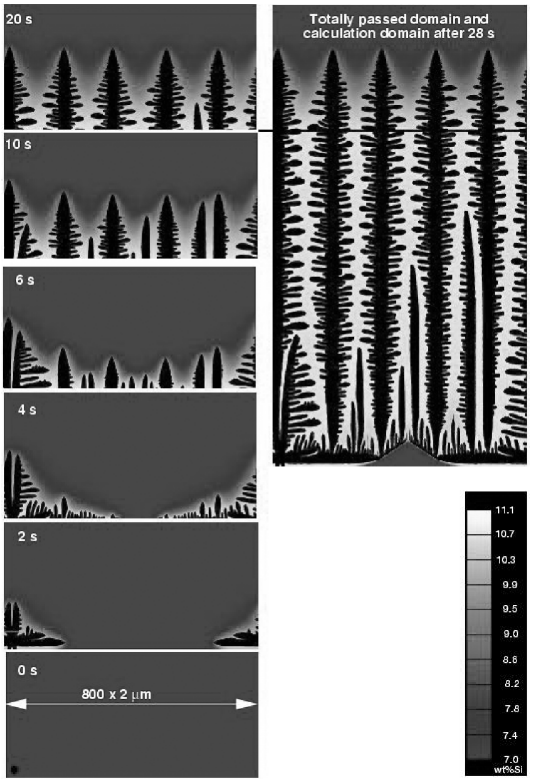

Fig. 1. Simulation of dendritic growth and selection of primary spacing in directional solidification of Al–7%Si in a moving frame of reference. Concentration in solid is darkened. The left side shows the time evolution of the moving calculation domain, while the right side shows also parts below the calculation domain itself, which have been "frozen-in" in the totally calculated domain. Side-branches are provoked by numerical instabilities.

concentration and phase-field values. The rows falling out of the moving "calculation domain" were stored in an extra file, describing finally a "frozen-in domain". The procedure can be understood looking at Fig. 1, showing on the left side several time steps of the moving calculation domain and on the right side the totally "passed" domain.

3. Simulations

The lay-out of a first calculation was due to a directional solidification experiment at ACCESS e.V. with Al–Si7 [18]. In Table 1 solidification conditions, material data and also numerical parameters are summarized. Solute diffusion in solid was neglected. In east–west direction we applied periodic boundary conditions, isolation at the bottom and a fixed concentration (7%) at the top. The attachment kinetics was assumed to have a four-fold asymmetry of 60%. Explicit noise was not set in the calculations.

The simulation result shown in Fig. 1 started from one seed splitting in the initially undercooled melt directed to the preferred crystal orientation. Then ternary arms build up a dense array of primary arms in direction against the heat flow. While the speed of the tips is retarded from the fast initial growth to the final speed imposed by the temperature profile, the primary spacing selects finally to 320 μm.

Fig. 2 compares the pattern formation for different initial seed densities, while all other conditions are the same as in Fig. 1. As the start from one or two initial seeds results in a spread out of number of truncs up to a minimal spacing of 260 μm, the start from three or four seeds results in spacings up to 530 μm.

The calculated range of dendritic spacings from 260 to 530 μm is close to the experimental finding of $\lambda_{\mathrm{exp}} = 250\,\mu\mathrm{m}$, though this comparison is difficult because of the two-dimensionality and numerical distortions. For additional comparison Eq. (1) provides us with $\lambda_{\mathrm{th}} = 62\,\mu\mathrm{m}$, which is much smaller than the simulation results.

Fig. 3 finally shows the sequence of the evolving microstructure calculated with variation of the cooling rate $R(t)$ during the calculation in sinus form as an imposed variation of the temperature distribution

$$R(t) = R_{\mathrm{average}} + \mathrm{A}\sin(2\pi t/P)$$

with $R_{\mathrm{average}} = 1.66\,\mathrm{K/s}$ as before. The amplitude is $A = 1.3\,\mathrm{K/s}$ and the period $P = 400\,\mathrm{s}$ (compare Fig. 4). This period was a compromise between the time necessary to reach quasistationary changes of the solidification speed and available computation time. Now the time-dependent individual front evolution changes everytime, while the so resulting morphology type changes quasistationarily due to the relatively slow changing growth conditions.

Table 1
Material, process, numerical data used for Al–7%Si

Alloy concentration	$c_0 = 7$	wt%
Melting temp.	$T_{\mathrm{m}}(c_0) = 855$	K
Liquidus slope	$m_l = -6$	K/wt%
Distribution	$k = 0.13$	
Diffusion	$D = 3 \times 10^{-9}$	$\mathrm{m^2/s}$
Gibbs–Thomson	$\Gamma = 2 \times 10^{-7}$	K m
Interface thickness	$\delta = 6\Delta x = 12$	μm
Attachment kinetics	$\mu = 0.32$	mm/sK
Anisotropy	$\Delta_\mu = 0.6$	
Temp-gradient	$G = 20$	K/mm
Cooling rate	$R = 1.66$	K/s

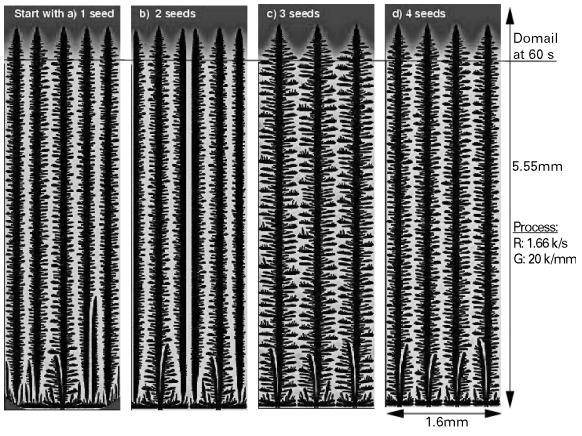

Fig. 2. Variation of initial seed spacing during dendritic growth simulation of Al–7%Si. The picture corresponds to the right side of Fig. 1. Depending on the initial seed density different primary spacings select out. For comparison first experiments provided us with $\lambda_{\mathrm{exp}} = 250\,\mu\mathrm{m}$ and theory gives $\lambda = 62\,\mu\mathrm{m}$.

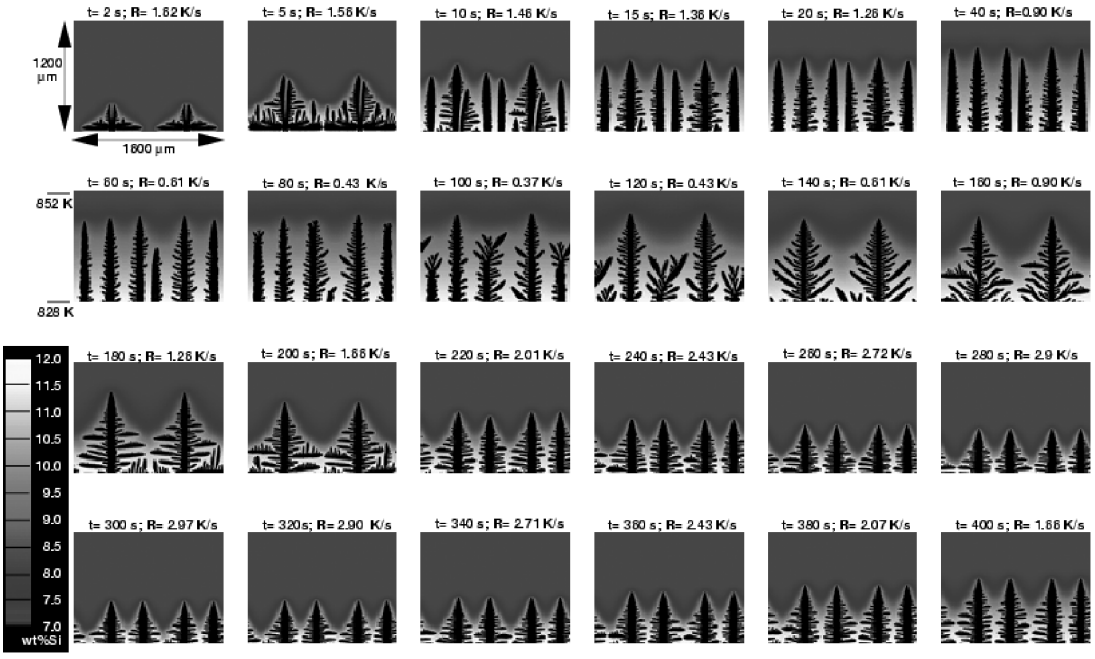

Fig. 3. Variation of the cooling rate during directional dendritic growth simulation of Al–7%Si. The time sequence shows the system reactions like changing tip-undercooling and changing primary spacing qualitatively. Decreasing growth rates (from 0 to 100 s) lead to extinction of redundant truncs. Acceleration leads again to birth of new primary truncs from ternary arms. The delay observed here is so strong, that even for doubling the original speed it does not reproduce the original. This history-dependent selection behaviour fits qualitatively with newer theories and experimental observations. Side-branches in diagonal direction are due to numerical anisotropy.

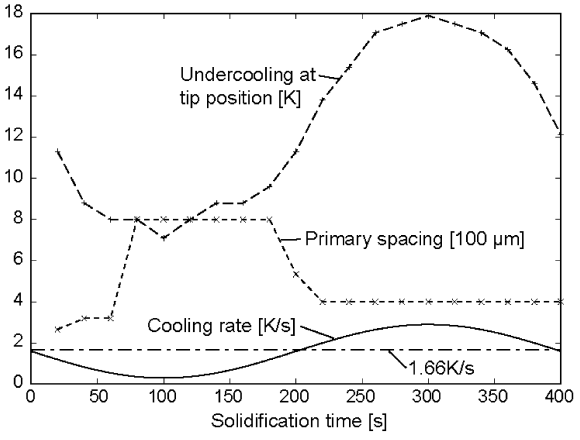

Fig. 4. Tip-undercooling, primary spacing as reaction on time-dependent variation of the cooling rate due to Fig. 3.

Starting with 2 seeds, the selection behaviour during the first time is quite similar to the correspondent set in Fig. 3 with constant cooling rate. With decreasing cooling rate the diffusion length becomes longer, the tip undercooling is reduced and the first primary trunks die out. At the minimum cooling rate only two primary trunks remain. For this slow velocity there is still the question, if steady state is already reached.

At low speed we observe also side branching in diagonal direction, which is absolutely due to numerical anisotropy concurring with the given anisotropy in the attachment kinetics in main direction. As kinetics plays less role at slow velocities, numerical anisotropy becomes obviously dominant in this regime and vanishes again for higher speeds. In this discussion it is good to know, that the side branching in the actual simulations originates from remaining phase-field instabilities using a coarse numerical grid.

The following acceleration on the one side leads to higher tip undercoolings again. The diffusion fields around the tips form deep grooves, so that finally the ternary arms can invade in highly

undercooled regions leading to birth of new primary truncs. This event happens when the cooling rate of the start is recovered. Further acceleration does not lead to further birth in the actual simulations, even the primary spacing provoked by the initial conditions is not reached. The time-varying values for cooling rate, tip undercooling and primary spacing are also included in Fig. 4. Because of the numerical distortions and model problems these results should not be considered to be fully quantitative, but they give a qualitative picture close to reality. In future validation and implementation of more advanced phase-field models like as given in Ref. [14] should be tested in comparison to experimental work.

Acknowledgements

This work is financially supported by the Deutsche Forschungsgemeinschaft (DFG) under Grant Nr. He 2700/6-1 and by the German Aerospace Center (DLR) under Grant Nr. 50WM 0043.

References

[1] J.D. Hunt, in: Solidification and Casting of Metals, The Metals Society, Book 192, London 1997, p. 3.
[2] W. Kurz, D.J. Fisher, Acta. Metall. 29 (1981) 11.
[3] D. Ma, P.R. Sahm, Metall. Mater. Trans. 29 A (1998) 1113.
[4] J.A. Warren, J.S. Langer, Phys. Rev. A 42 (1990) 3518.
[5] J.A. Warren, J.S. Langer, Phys. Rev. E 47 (1993) 2702.
[6] W.D. Huang, W.G. Geng, Y.H. Zhou, J. Crystal Growth 134 (1993) 105.
[7] H. Weidong, G. Xingguo, Z. Yaohe, J. Crystal Growth 134 (1993) 105.
[8] X. Lin, W.D. Huang, J. Feng, T. Li, Y. Zhou, Acta Mater. 47 (11) (1999) 3271.
[9] J. Tiaden, B. Nestler, H. Diepers, I. Steinbach, Physica D 115 (1998) 73.
[10] A.A. Wheeler, W.J. Boettinger, G.B. McFadden, Phys. Rev. A 45 (1992) 7424.
[11] J. Warren, W.J. Boettinger, Acta Metall. Mater. 43 (2) (1995) 689.
[12] S.G. Kim, et al., Phys. Rev. E 60 (6) (1999) 1.
[13] R.F. Almgren, SIAM J. Appl. Math 59 (1999) 2086.
[14] A. Karma, Cond-Mat/0103289, 2001, preprint.
[15] S.V. Patankar, Numerical Heat Transfer and Fluid Flow, Hemisphere, Washingtion DC, 1980.
[16] C. Beckermann, H. Diepers, I. Steinbach, A. Karma, X. Tong, J. Comp. Physics 154 (1999) 468.
[17] S. Wang, et al., Physica D 69 (1993) 189.
[18] A. Weiß, H.-J. Diepers, G. Zimmermann, Progress report: Dendritic Solidification, Contribution to ESA AO-99-031/ MICAST, ACCESS e.V. 2001.